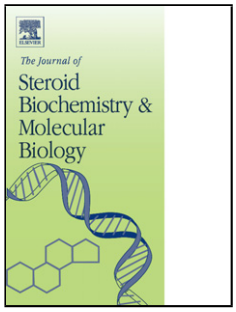


Title: The UVB1 Vitamin D Analogue Inhibits Colorectal Carcinoma Progression

Author: María Julia Ferronato Eliana Noelia Alonso Norberto Ariel Gandini María Eugenia Fermento María Emilia Villegas Mario Alfredo Quevedo Julián Arévalo Alejandro López Romero Marcos Lois Rivadulla Generosa Gómez Yagamare Fall María Marta Facchinetti Alejandro Carlos Curino

PII: S0960-0760(16)30149-2
DOI: http://dx.doi.org/doi:10.1016/j.jsbmb.2016.05.019
Reference: SBMB 4734

To appear in: *Journal of Steroid Biochemistry & Molecular Biology*

Received date: 3-3-2016
Revised date: 26-4-2016
Accepted date: 17-5-2016

Please cite this article as: María Julia Ferronato, Eliana Noelia Alonso, Norberto Ariel Gandini, María Eugenia Fermento, María Emilia Villegas, Mario Alfredo Quevedo, Julián Arévalo, Alejandro López Romero, Marcos Lois Rivadulla, Generosa Gómez, Yagamare Fall, María Marta Facchinetti, Alejandro Carlos Curino, The UVB1 Vitamin D Analogue Inhibits Colorectal Carcinoma Progression, Journal of Steroid Biochemistry and Molecular Biology http://dx.doi.org/10.1016/j.jsbmb.2016.05.019

*Study of the effects of UVB1 on colorectal cancer*

# The UVB1 Vitamin D Analogue Inhibits Colorectal Carcinoma Progression

María Julia Ferronato[1], Eliana Noelia Alonso[1], Norberto Ariel Gandini[1], María Eugenia Fermento[1], María Emilia Villegas[1], Mario Alfredo Quevedo[2], Julián Arévalo[3], Alejandro López Romero[4], Marcos Lois Rivadulla[5], Generosa Gómez[5], Yagamare Fall[5], María Marta Facchinetti[1], Alejandro Carlos Curino[1*].

1. Laboratorio de Biología del Cáncer, Instituto de Investigaciones Bioquímicas Bahía Blanca, Centro Científico Tecnológico Bahía Blanca (INIBIBB-CONICET), Bahía Blanca, Argentina.

2. Unidad de Investigación y Desarrollo en Tecnología Farmacéutica (UNITEFA-CONICET), Facultad de Ciencias Químicas, Ciudad Universitaria, Universidad Nacional de Córdoba, 5000 Córdoba, Argentina.

3. Servicio de Patología del Hospital Interzonal General de Agudos Dr. José Penna, Av. Láinez 2401, 8000 Bahía Blanca, Argentina.

4. Departamento de Hematología, Laboratorios IACA, Bahía Blanca, Argentina.

5. Departamento de Química Orgánica, Facultad de Química and Instituto de Investigación Biomédica (IBI), University of Vigo, Campus Lagoas de Marcosende, 36310 Vigo, Spain.

* Laboratorio de Biología del Cáncer, Instituto de Investigaciones Bioquímicas Bahía Blanca (INIBIBB-CONICET), Centro Científico Tecnológico Bahía Blanca, Camino La Carrindanga. Km 7 - C.C. 857, 8000 Bahía Blanca, Argentina; Tel: (54) 291-4861201 ext. 130; Fax: (54) 291-4861200; E-mail: acurino@criba.edu.ar.

## Highlights

►UVB1 induces apoptotic cell death of HCT116 colorectal carcinoma cells.

►UVB1 inhibits cellular migration and invasion in colorectal carcinoma cell line.

►UVB1 increases E-cadherin and VDR expression in HCT116 cell line.

► UVB1 reduces tumour volume of a xenograft murine model of colorectal cancer.

►UVB1 exhibits greater affinity for the VDR ligand binding domain than calcitriol.

## ABSTRACT

Vitamin D has been shown to display a wide variety of antitumour effects, but their therapeutic use is limited by its severe side effects. We have designed and synthesized a Gemini vitamin D analogue of calcitriol (UVB1) which has shown to display antineoplastic effects on different cancer cell lines without causing hypercalcemia. The aim of this work has been to investigate, by employing *in silico*, *in vitro*, and *in vivo* assays, whether UVB1 inhibits human colorectal carcinoma progression. We demonstrated that UVB1 induces apoptotic cell death and retards cellular migration and invasion of HCT116 colorectal carcinoma cells. Moreover, the analogue reduced the tumour volume *in vivo*, and modulated the expression of Bax, E-cadherin and nuclear β-catenin in tumour animal tissues without producing toxic effects. *In silico* analysis showed that UVB1 exhibits greater affinity for the ligand binding domain of vitamin D receptor than calcitriol, and that several characteristics in the three-dimensional conformation of VDR may influence the biological effects. These results demonstrate that the Gemini vitamin D analogue affects the growth of the colorectal cancer and suggest that UVB1 is a potential chemotherapeutic agent for treatment of this disease.



## KEYWORDS

Colorectal cancer; Analogue; Calcitriol; Vitamin D; Gemini

## 1. INTRODUCTION

Vitamin D is a prohormone responsible for maintaining calcium and phosphate homeostasis. It is metabolized in the liver and kidney to produce the active form of vitamin D, named calcitriol [1]. This active form has been shown to regulate most of the capabilities that cancer cells acquire in their progression to a malignant state and metastatic dissemination. These capabilities named the "hallmarks of cancer" [2] are: sustaining proliferative signaling, evading growth suppressors, resisting cell death, enabling replicative immortality, inducing angiogenesis, activating invasion and metastasis, altering genome stability, inducing inflammation, reprogramming energy metabolism and evading immune destruction [3,4]. Calcitriol regulates these processes either through genomic and/or non-genomic pathways [4-6]. The genomic effects produced by calcitriol are mediated by the Vitamin D Receptor (VDR), a member of the nuclear receptor family that exhibits a ligand-dependent transcriptional regulation [7]. Human VDR, which consists of 427 amino acids, comprises two core functional domains: the DNA binding domain (DBD) and the ligand binding domain (LBD), both connected through a hinge region. The LBD region is formed by 12 α helices (H1-H12) and 3 β sheets [8]. Activation of VDR is highly dependent on the ability of ligands to produce an allosteric control on the LBD by eliciting a conformational modulation of the H12 helix, the so-called functional activated domain AF-2 which, in turn, mediates the binding of transcriptional co-modulators, leading to the corresponding biological events [9]. As expected, the binding site of VDR agonists is located in the proximity of the H12 helix, where crucial intermolecular interactions are likely to be established.

Colorectal cancer (CRC) is the third most commonly diagnosed cancer in males and the second in females, and ranks as the third leading cause of cancer mortality worldwide [10,11]. CRC develops through a multistep process in which normal mucosa first transitions to adenomatous polyps and then eventually to invasive carcinoma. Approximately 40–50% of patients diagnosed with CRC will develop distant metastases. In spite of improved survival of patients with metastatic colorectal cancer by treatment with chemotherapy over the last decade [12], it is however necessary to find new targeted therapies that block the growth and spread of this cancer type.

Vitamin D compounds have been shown to modulate CRC initiation and progression, interacting with Wnt/β-catenin signaling and the innate immune response [13,14]. Nevertheless, the use of calcitriol is restricted by its hypercalciuria and hypercalcemic effect at therapeutic doses [15]. This can be putatively overcome by the use of analogues that retain the antitumour action but have less calcemic effects.

We have previously reported the synthesis of a novel Gemini vitamin D analog, named UVB1, which has two side chains in C-20 and demonstrates potent antitumour effects over a wide panel of tumour cell lines and lacks hypercalcemic activity in mice [16]. In the present study, we have investigated, by employing *in vitro* and *in vivo* assays, whether UVB1 inhibits human colorectal carcinoma progression. By applying state-of-the-art molecular modeling techniques we have also studied the intermolecular interaction between UVB1 and VDR and the corresponding structural effects on AF-2.

## 2. MATERIALS AND METHODS

### *2.1. Chemicals and Reagents*

1α,25-dihyroxyvitamin $D_3$ (calcitriol) and UVB1 were reconstituted as previously described [16]. Briefly, the compounds were dissolved in 100% HPLC-grade isopropanol (vehicle) and stored protected from light at –20°C. The calcitriol and UVB1 concentrations were determined by UV spectrophotometry between 200 and 300 nm. Both compounds were diluted in the culture medium to reach the required concentrations. The maximal concentration of vehicle used in this study had no effect on cell growth, migration and invasion.

*2.2. Cell lines*

Biological evaluation of UVB1 was performed in the human HCT116 and HCT116 p53-/- colorectal carcinoma cell lines. Cells were maintained at 37°C, 5% $CO_2$ in DMEM supplemented with 100 U/ml penicillin, 100 U/ml streptomycin, 4 mM glutamine and 10% FBS.

*2.3. Cell Count and Viability Assay*

For the dose - time - course response analysis, the HCT116 cells were plated at a density of 500 cells/well into 96 multi-well plates in complete medium, and treated with 0.01 to 100 nM of UVB1 or vehicle. The cells were incubated for 24, 48, 72, 96 and 120 h. Following treatments, cellular viability was assessed by the WST-1 colorimetric assay (Roche, Argentina). The cells were incubated for 1 h with the tetrazolium salt (4-[3-(4-Iodophenyl)-2-(4-nitrophenyl)-2H-5-tetrazolio]-1,3-benzenedisulfonate) and the formazan product determined by absorbance reading at 440 nm. The reference wavelength was 690 nm. Then the cells were washed with PBS, trypsinized and suspended in complete medium (100 µl) and counted manually using a hemocytometer.

HCT116 p53-/- cells were seeded into 96 multi-well plates in complete medium, and treated with 0.01 to 100 nM of calcitriol, UVB1 or vehicle. The medium was replaced every 2 days and the cells were incubated for 120 h. They were then washed with PBS 1X, trypsinized and suspended in complete medium (100 µl) and counted manually using a hemocytometer. Additionally, the results were checked by the WST-1colorimetric assay.

*2.4. Cell Cycle Analysis by Flow Cytometry*

For fluorescence-activated cell sorting (FACS) analysis, HCT116 cells were plated at a density of 100,000 cells per 100 mm dish in DMEM supplemented with 10% FBS. Twenty-four hours after plating, cells were treated with UVB1, calcitriol or vehicle (1 nM) during 120 h. Then, cells were harvested by trypsinization washed twice with ice-cold 1X PBS, fixed by 70% ethanol and incubated at -20° C during 24 h. Before flow cytometry analysis, the cellular double-stranded nucleic acids were stained with propidium iodine (PI) (Roche, 50 $\mu g.ml^{-1}$) and RNase A (100 $U.ml^{-1}$) to degrade double-stranded RNA in PBS

for 60 min at room temperature. Cell cycle analysis was performed with FACScan flow cytometry (Becton Dickinson). Data were analysed using Cell Quest software (Becton Dickinson, Heidelberg, Germany). One thousand forward scatter gated events were collected per sample.

*2.5. TUNEL assay*

Cells were seeded onto coverslips at a density of 50,000 cells per 35 mm dish and after 24 h they were treated with UVB1, calcitriol or vehicle (100 nM) during 72 h. Then the cells were fixed with 4 % formaldehyde in PBS for 60 min at room temperature, washed with PBS twice for 5 min and incubated with blocking solution (3% $H_2O_2$ in methanol) during 10 min. After that, coverslips were washed with PBS twice for 5 min and coated with permeabilisation solution (0.1% Triton X-100 in 0.1% sodium citrate, freshly prepared) and the In Situ Cell Death Detection Kit, POD (Roche) was employed to detect apoptotic cells. Photographs were taken using an inverted phase microscope NIKON ECLIPSE TE 2000S. Ten fields per condition were evaluated.

*2.6. Wound-Healing Assay*

HCT116 cells ($2.5 \times 10^5$) were seeded onto sterile 35 mm plates and allowed to grow until a confluent cell monolayer was formed. Wound healing assay was performed as previously described [17]. Cells were scratched with 200 µl pipette and then fresh medium containing UVB1, calcitriol or vehicle 100 nM was added to each plate. The photographs were taken at 0 and 18 h after scratching. Images were recorded with a microscope NIKON ECLIPSE TE 2000S. The area of the scratches was quantified using Image J Analysis software.

*2.7. Western blot analysis*

After treating the HCT116 cells with UVB1, calcitriol or vehicle, they were lysed in lysis buffer containing 2% TRIS 1M, 1% Triton-X 100, 0.5 M EDTA 0.5 M, 2% sodium chloride 1M for 30 min on ice and the protein concentration was determined by Bradford assay by using a Jasco V-630 spectrophotometer. Lysates were prepared to examine the expression of Bax (N-20, sc-493, 1:100; Santa Cruz Biotechnology), Cyclin D1 (SR4, 1:1,000; Thermo Scientific), Cyclin E (M-20, sc-481, 1:500; Santa Cruz Biotechnology),

VDR (1:750; Santa Cruz Biotechnology), E-cadherin (H-108, sc-7870, 1:500; Santa Cruz Biotechnology) and β-catenin (H-102, sc-7199, 1:1,000; Santa Cruz Biotechnology). The same amount of protein was separated by SDS-PAGE and transferred to PDVF membranes (Millipore). Membranes were subsequently blocked for 30 min at room temperature and further incubated at 4°C overnight with primary antibodies. Then, membranes were washed and incubated with the appropriate HRP-conjugated secondary antibodies (Santa Cruz Biotechnology) for 90 min at room temperature. Protein bands were visualized using the enhanced chemiluminescence method. Relative protein levels were calculated by normalization to the amount of actin protein (C-11, sc-1615, 1:1,000; Santa Cruz Biotechnology). Data shown are representative of three independent experiments.

*2.8. Immunofluorescence*

Immunofluorescence (IF) was performed as previously described [17]. Briefly, HCT116 cells were seeded on glass coverslips in 35 mm petri dishes and cultured until 50% confluence. They were treated with UVB1, calcitriol or vehicle for 96 h at 100 nM. After treatment, they were washed three times with PBS and fixed with paraformaldehyde (PFA) 4% in PBS. The cells were then permeabilized with 0.2 % triton in PBS and blocked with 1% BSA in PBS. Then they were incubated with E-cadherin (1:100, Santa Cruz Biotechnology) in 1% BSA in PBS for 1 h. After incubation with the primary antibody, the cells were washed with PBS and incubated with anti-rabbit Alexa 566 fluoro-conjugated antibodies (Molecular Probes, Invitrogen) for 1 h. Then they were washed and mounted. The cell nucleus was stained with DAPI (1:10,000). The cells with expression of E-cadherin were counted by analysing 10 images randomly for each condition.

*2.9. Animal Model and Treatments*

All animal experiments followed the guidelines of the Committee for the Care and Use of Laboratory Animals of the NIH and of the local committee. Twelve animals were used in the xenograft model. Male N:NHI (S)- *Fox1* $^{nu}$ mice, 25 g, 10 weeks old were purchased from the Facultad de Ciencias Veterinarias (La Plata, Argentina). The animals were housed under pathogen-free conditions, in plastic cages, under controlled temperature and

humidity, with a 12:12 hr light–dark cycle and free access to food and water. Animals were acclimatized for at least one week before use.

The tumour xenograft model was employed to assess antitumour activity of UVB1. HCT116 cells ($5 \times 10^6$) [18] were implanted subcutaneously in the backs of mice. When the diameter of tumour mass was 5 mm (approximately seven days following cell inoculation), animals were randomized in two groups and injected subcutaneously in the backs of mice with UVB1 (n=6) and vehicle (n=6) at 40 $\mu g.kg^{-1}$ three times a week during four weeks. Tumour growth was blindly measured daily with calipers, and tumour volume was calculated as $\pi/6 \times a \times b^2$, where *a* is the length in millimeters, and *b* is the width in millimeters. At the end animals were sacrificed by cervical dislocation. Tumours were then removed, weighed, measured and put into formaldehyde for further hematoxylin and eosin (H&E) or immunohistochemical studies. Tumour volume was calculated as $\pi/6 \times a \times b \times c$, where *a*, *b*, and *c* are the three tumour dimensions.

After tumour paraffin sections were dewaxed, they were rehydrated in a series of ethanol dilutions and either stained with H&E or used for immunohistochemical studies. Mitotic index was calculated as the number of the mitotic figures observed in 10 fields at a magnification of ×400 in the H&E stained slides. Also, the percentage of necrotic cells was calculated.

*2.10. Immunohistochemical Staining*

IHC was performed by using the avidin-biotin complex immunoperoxidase technique. Five μm sections of paraffin-embedded specimens were mounted on glass slides, deparaffinized with xylene, and rehydrated with graded alcohol. They were incubated for 15 min in 3% hydrogen peroxide in ethanol at 96 °C to quench endogenous peroxidase. After washing in PBS 1X, the sections were blocked for 30 min in 2% bovine serum albumin (BSA, in PBS 1X) and then incubated overnight at 4 °C with primary antibodies. After that, they were incubated with diluted biotinylated secondary antibody for 30 min and then incubated with Vectastain ABC reagent (Vector Laboratories Inc.) for 30 min. Diaminobenzidine/H2O2 were used as substrates for the immunoperoxidase reaction. They were lightly counterstained with Harris Hematoxylin (Zymed Laboratories), dehydrated through graded ethanol and xylene, mounted with Permount (Fisher Scientific) for analysis by bright field

microscopy, and examined under an Olympus microscope (CX31). For negative controls, the slides were subjected to the same IHC process omitting the primary antibody. Primary antibodies used were goat polyclonal anti-Ki-67 (M-19, sc-7846, dilution 1/100) with antigen retrieval, rabbit polyclonal anti-Bax (N-20, sc-493, dilution 1/100), rabbit polyclonal ant-E-cadherin (H-108, sc-7870, dilution 1/100) and β-catenin (H-102, sc-7199, dilution 1/250) from Santa Cruz Biotechnology.

Immunostained sections were scored semiquantitatively based upon the proportion of tumour cells stained and the staining intensity, using the Immuno-Reactive-Score (IRS) system as suggested by Remmele and Stegner [19]. Expression was evaluated as previously described [20]. The IRS was calculated as the product of the staining intensity (graded as: 0= no, 1= weak, 2= moderate and 3 = strong staining) by the percentage of positively stained cells (0 = less than 10% of stained cells, 1 = 11–50% of stained cells, 2 = 51–80% of stained cells and 3 = more than 80% of stained cells). The mean IRSs for Bax , E-cadherin and β-catenin in ten randomly chosen fields of the sample (×400 magnification) were determined. Ki-67 expression was calculated by the percentage of positively stained cells (0 = less than 10% of stained cells, 1 = 11–50% of stained cells, 2 = 51–80% of stained cells and 3 = more than 80% of stained cells). All samples were evaluated and scored simultaneously by a pathologist (JA) and two investigators (NG and EA), all of them blind to sample information.

*2.11. Blood Calcium Levels*

Animals were treated with 40 $\mu g.kg^{-1}$ body weight of UVB1 or vehicle (n= 6 per group). Blood samples were collected from mice at the beginning and at the end of the experiments. Animals were anesthetized as described previously [17] and capillary tubes were used to collect blood from the retro-orbital sinus. Samples were held on ice, processed at 4°C, and plasma was separated and stored at –20°C until assayed. Approximately 40µl of plasma/mouse was obtained. Calcium concentration was determined using Ca-Color Arsenazo III AA kit (Wiener Lab, Argentina), measuring the absorbance at 650 nm; the sample calcium concentration was calculated based upon calcium standards provided by the manufacturer. Additionally, the hematocrit for each mouse was analysed before and following treatments to determine if the mice were

healthy. General toxicity was assessed by clinical measures, such as weight loss, changes in appearance and behavior, lethargy and death. Animal weight was evaluated three times a week.

*2.12. Liver, Kidney and Spleen Histological Analysis*

Dissected livers, kidneys and spleens from animals treated with UVB1 and vehicle were fixed in 10% saline formalin during 24 h and gradually dehydrated using serial ethanol concentrations of 70%, 90%, and 100%. Dehydrated organs were cleared for two h using xylol and then included in paraffin. Sections (5 µm thick) were prepared using a rotary microtome (Leica, RM 2155), attached to clean slides and stained with H&E for histological examination by an expert pathologist (JA). For each slide, 10 fields at ×100 and ×400 magnification were analysed.

*2.13. Molecular modeling studies*

Computational studies were performed using as reference the crystallographic structure of the calcitriol-VDR complex (pdb code: 1DB1) [7] previously deposited in the Protein Databank [21]. The X-ray receptor model used as template structure for the *in silico* studies was carefully selected among the available X-ray crystal structures taking into account the quality, performance and structural validation of deposited structures [22]. From these analyses it was concluded that the structure deposited in the Protein Databank by Rochel et al. under the code 1DB1, constitutes a sufficiently validated model. Initial structures of calcitriol and UVB1 were built using the MarvinSketch software [23], after which structural and energetic analyses were performed using the Gaussian03 [24] software in order to obtain the minimum energy conformation by applying semiempirical (AM1) and ab initio (HF/6-311+G*) methods.

Molecular docking assays were performed using software packages developed by OpenEye Scientific Software. Docking procedures consisted of three sequential stages: a) a ligand conformer library generation, which was conducted at an energy threshold of 10 kcal/mol using the OMEGA software [25,26], b) the docking runs, which were performed by applying a fast rigid exhaustive docking approach as implemented in the FRED3 software [27-29] with the ChemGauss3 scoring function being used to evaluate and rank resulting docked poses. The lowest energy docked pose was considered for further analyses. Stage

c) involved three dimensional visualization and intermolecular interactions predictions, which were performed using the VIDA [30] and LigPlot+ [31] software packages, respectively.

The *AMBER14* software package [32,33] was used to obtain and analyse molecular dynamics (MD) trajectories. Atomic charges and molecular parameters corresponding to calcitriol and UVB1 were assigned from the *GAFF* force field [34], while those corresponding to the macromolecule were assigned from the AMBER force field 99SB [35]. To obtain MD trajectories, the complexes predicted by molecular docking were used as initial structures, solvated with a pre-equilibrated TIP3P octahedral box of explicit water molecules, and subjected to energy minimization. The minimized systems were heated to 298 K for 100 ps, using a time step of 2 fs under constant pressure and temperature conditions. The SHAKE algorithm was applied to constrain bonds involving hydrogen atoms. After concluding the heating phase, an equilibration stage (1 ns) was performed and followed by the corresponding production stages (20 ns). Analyses of the MD trajectories were carried out using the *Cpptraj* module of *AMBER14*, with energetic and per-residue decomposition analyses being performed by applying the molecular mechanics Poisson−Boltzmann surface area (MM-PBSA) approach as implemented in the MMPBSA.py tool [36]. The resulting trajectories were visualized using *VMD v.1.9* software [37].

In all cases, MD trajectories were obtained using CUDA designed code (*pmemd.cuda*), with computational facilities provided by the GPGPU Computing group at the Facultad de Matemática, Astronomía y Física (FAMAF), Universidad Nacional de Córdoba, Argentina.

*2.14. Statistical Analyses*

GraphPad Prism 5.0 software package was used for all statistical analyses. To establish whether or not each parameter group represented a normal distribution, a D'Agostino–Pearson Omnibus normality test was performed. Viability and flow cytometry data were analysed using two way ANOVA with Bonferroni posttest analysis. Wound healing assays, invasion assays, TUNEL assay, differences in E-cadherin expression between UVB1, calcitriol and vehicle were analysed using one way ANOVA with Bonferroni's Multiple Comparison Test. Comparison of the tumour volume *in vivo* and *ex vivo* statistical

significance was evaluated using two way ANOVA with Bonferroni posttest and student's t test, respectively. Mitotic index, percentage of necrosis and immunohistochemical staining were analysed by the non-parametrical Mann– Whitney U test. Effects on plasma calcium levels and hematocrit of the animals were analysed by unpaired t test. A p value <0.05 was considered significant.

## 3. RESULTS

### *3.1. UVB1 induces apoptotic cell death of HCT116 colorectal carcinoma cells*

To evaluate the effects of the analogue on cellular viability we performed dose- and time-course response experiments over a total period of 120 h and with 0.01 to 100 nM concentrations of UVB1 in human colorectal carcinoma cell line (HCT116). As shown in figure 1A we observed a significant reduction in cell number at 96 h with the concentration of 100 nM of UVB1. Also, we confirmed our previous results showing that the analogue decreases cellular viability at 120 h with 0.1 to 100 nM concentrations [16].

Since the tumour suppressor p53 is important for the regulation of cellular survival and is frequently dysregulated in CRC, we performed similar experiments using the cell line HCT116 p53−/− which lacks p53 protein. Interestingly, the UVB1 analogue did not affect the viability of these cells with any of the doses tested. However, calcitriol maintained its effect on reducing cell viability. This suggests that UVB1 effects over cell survival is p53-dependent whereas calcitriol effects are not.

To further analyse if the reduction in cell number was due to an effect on cell proliferation or cell death, the cell cycle was studied by flow cytometry in HCT116 cells treated with UVB1 or calcitriol at 1 nM concentration ($IC_{50}$) for 120 h and labelled with PI. As depicted in figure 1C, UVB1 or calcitriol treatment caused an increase in the percentage of cells in sub $G_0/G_1$ phase compared to vehicle-treated cells. After UVB1 treatment the percentage of cells in sub $G_0/G_1$ phase was 50.69 ± 1.22% compared to 10.45 ± 1.675% in the vehicle-treated cells (*** $p< 0.001$); this increase of cells in sub $G_0/G_1$ phase was accompanied by a decrease of cells in $G_0/G_1$ population and S phase. Calcitriol induced an increase of cells in sub $G_0/G_1$ phase with a decrease in $G_2$/M. Of note, UVB1 produced a greater increase of cells in sub $G_0/G_1$ phase compared to calcitriol (50.69 ± 1.22% vs 17.40 ± 2.48%; p=

0.0003). Thus, UVB1 is three times more potent than calcitriol to cause HCT116 cell death.

In order to corroborate if this increase in sub $G_0/G_1$ population was due to an induction of apoptosis, TUNEL assay was performed after 72 h of UVB1 or calcitriol incubation at 100 nM concentration. As shown in figure 1D the treatment with the analogue produced an increase in the percentage of TUNEL positive cells respect to control (9.86 ± 1.01% vs 7.38 ± 0.38%; p= 0.026) while calcitriol did not produce an increase in TUNEL positive cells (7.57 ± 0.45% vs 7.38 ± 0.38%; p> 0.05).

These results are consistent with both the increase in the protein expression levels of Bax, a marker of apoptosis, observed after UVB1 treatment (figure 1E) and the absence of change in the cell cycle regulators cyclin D and cyclin E by western blot.

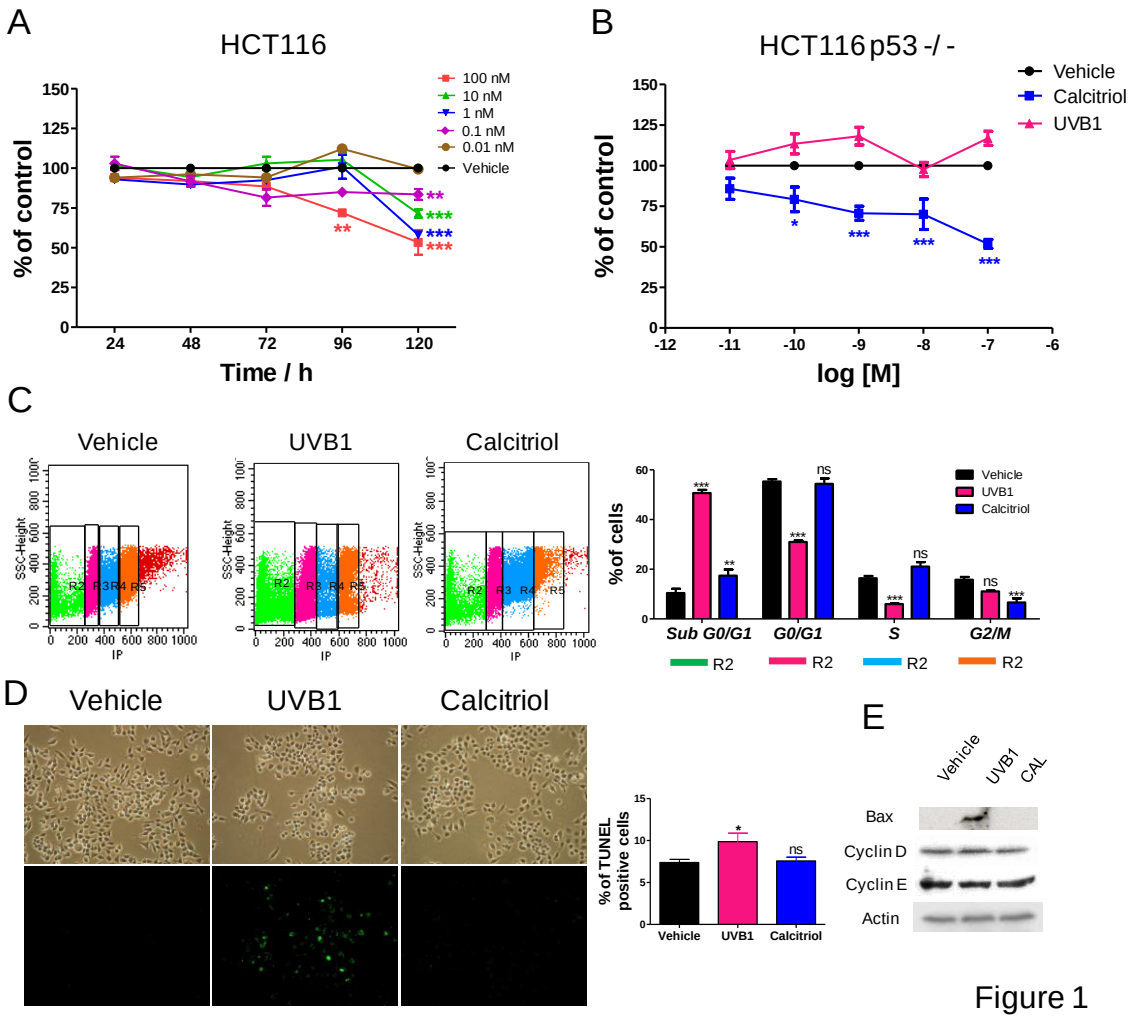


Figure 1

Figure 1. Study of the effects of UVB1 or calcitriol on cellular viability and cell cycle of human colorectal carcinoma cell lines. A) Dose – Time - course response analysis of UVB1 on cell viability of HCT116 cell line. B) Cell viability in HCT116 p53-/- cells after exposed to 0.01-100 nM concentrations of UVB1 or calcitriol over 120 h. Viability was expressed as percentage of the vehicle-treated cells. Data points represent means ± SEM from three independent assays. * $p< 0.05$, ** $p< 0.01$ and *** $p< 0.001$. C) Flow cytometry analysis in HCT116 cell line treated with UVB1 (1 nM; 120 h) and calcitriol (1 nM; 120 h) and stained with PI. D) TUNEL assay photomicrographs and its quantification of HCT116 cells treated with vehicle, UVB1 or calcitriol (100 nM; 72 h). E) Effect of UVB1 and calcitriol on Bax (100 nM, 96 h), cyclin D and cyclin E (1 nM; 96 h) by western blotting in HCT116 cell line.

### *3.2. UVB1 retards cell migration and invasion of HCT116 cell line*

Migration and invasion of tumour cells in the surrounding tissues is an important step in cancer progression and calcitriol and its analogues have shown to inhibit these processes in various tumour types [3,38]. Hence, we evaluated the effect of UVB1 on cell migration by a wound healing assay in the HCT116 cells, comparing the analogue effect with that exerted by calcitriol. HTC116 cells were grown to confluence, and following a wound production they were treated with the analogue, calcitriol or vehicle at 100 nM over 18 h. As shown in figure 2A, UVB1 reduced significantly HCT116 cell migration compared to the control cells (wound uncovered area: UVB1: 69.91 ± 4.51 vs vehicle: 48.66 ± 3.87; $p= 0.003$). No differences were found in the rate of migration between cells treated with calcitriol or vehicle.

Then we performed invasion assays using Matrigel-coated transwell inserts to extend the studies of UVB1 effects on the invasive potential of human colorectal carcinoma cells. As observed in figure 2B, UVB1 and calcitriol treatment significantly reduced the number of HCT116 invasive cells when compared with vehicle-treated cells (invasive cell number: UVB1: 77.23 ± 2.74, calcitriol: 84.93 ± 1.66 vs vehicle: 107.70 ± 4.21; $p< 0.001$).

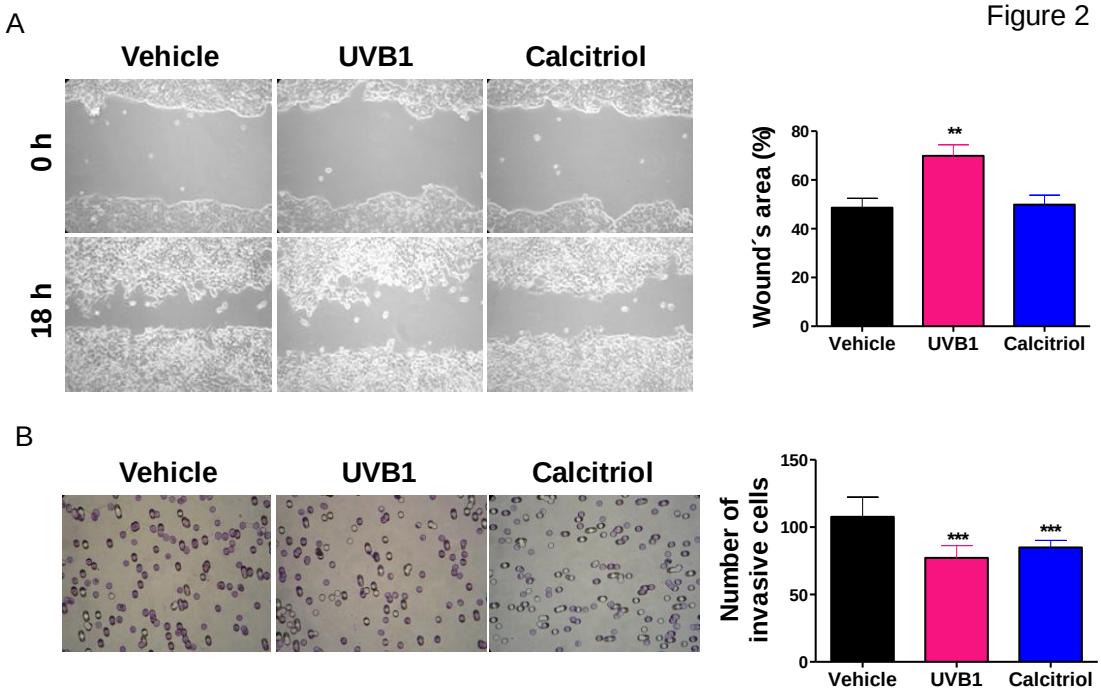


Figure 2. Evaluation of cellular migration and invasion following UVB1 or calcitriol treatment. A) Wound healing assay of the HCT116 cells treated with vehicle, UVB1 or calcitriol (100 nM, 18 h). The cells migrating into the scratched area were photographed (x200) and wound area was calculated as a percentage of migration. B) Cell invasion assay of the HCT116 cell line treated with vehicle, UVB1 and calcitriol (100 nM, 18 h). Each bar represents the average of 10 randomly chosen fields. Data are shown as the mean ± SEM of three independent experiments. * $p < 0.05$, ** $p < 0.01$ and *** $p < 0.001$.

### *3.3. UVB1 increases E-cadherin and VDR expression in HCT116 cell line*

Calcitriol and some of its analogues promote epithelial differentiation of human colon cancer cells by inducing the expression of E-cadherin and by antagonizing the Wnt/β-catenin pathway [39]. Additionally, it has been demonstrated that the binding of vitamin D receptor (VDR) to β-catenin precludes the formation of transcriptionally active β-catenin / T cell transcription factor (TCF) complexes in the cell nucleus [40]. Hence, we evaluated the expression of E-cadherin and VDR after the treatment of UVB1 or calcitriol in the HCT116 cell line. As shown in figure 3A the expression of E-cadherin was increased after UVB1 treatment as compared with vehicle treatment (38.32 ± 0.70 % vs 17.00 ± 5.70 %, $p = 0.012$). This was corroborated by western blot (figure 3B). Calcitriol did not produce differences in the expression of E-cadherin when compared with the control (23.01 ± 8.61 % vs 17.00 ± 5.70 %; $p > 0.05$). Also, UVB1 produced an increase in VDR expression

when compared to control treatment while no changes were observed with calcitriol treatment (figure 3B).

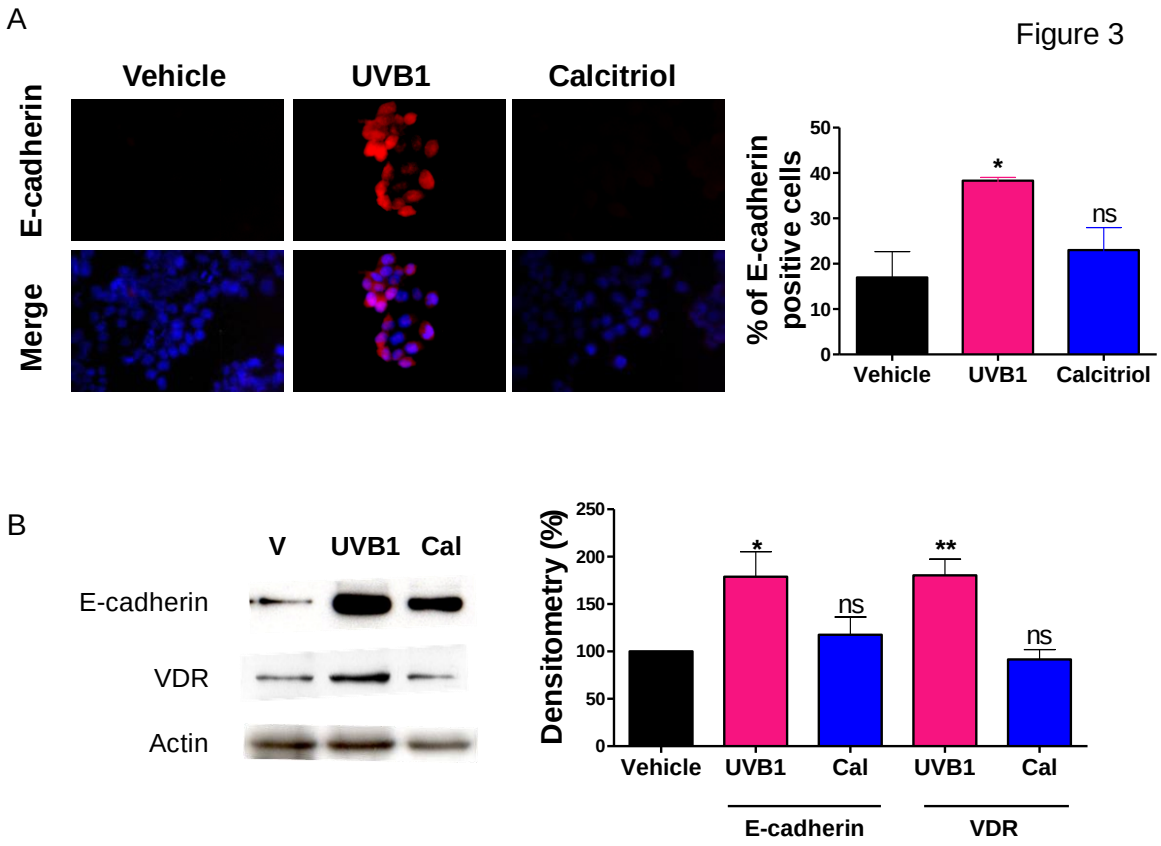


Figure 3

Figure 3. Study of the effect of UVB1 or calcitriol on E-cadherin and VDR expression. A) E-cadherin expression in HCT116 cell line by IF. The cells were treated with UVB1, calcitriol or vehicle over 96 h. Each bar represents the average of 10 randomly chosen fields. * $p< 0.05$. B) E-cadherin and VDR expression by western blot. The blots correspond to one representative experiment. The graph shows the densitometry of bands. The experiments have been performed three independent times. Protein loading was normalized with actin.

### *3.4. UVB1 reduces the tumour volume in a xenograft murine model of colorectal cancer*

To evaluate the antitumour effects of UVB1 *in vivo*, we studied the effect of this analogue on the primary tumour growth in a HCT116 xenograft animal model. The N:NIH(S)-*Fox1*$^{nu}$ mice were treated with UVB1 or vehicle (40 µg.kg$^{-1}$ body weight) during four weeks. In figure 4A, the evolution of tumour growth in both groups during the time of drug

administration is shown. UVB1 reduced the tumour volume significantly; the *ex vivo* tumour volume of the vehicle group was 2563 ± 703 $mm^3$ while that of UVB1 group was 916 ± 153 $mm^3$; p= 0.045 (figure 4B).

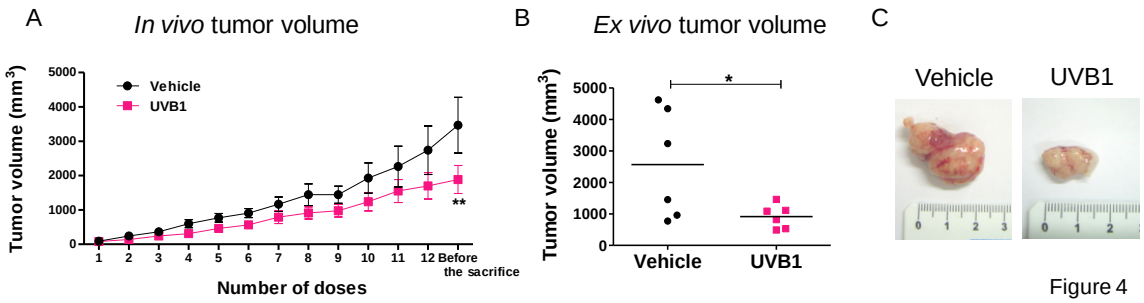


Figure 4

Figure 4. Tumour growth of HCT116 xenograft animal model following treatment with UVB1. A) *In vivo* tumour volume was calculated with the following equation: ($A^2$ x B) x π/6, A: width; B: length. ** p< 0.01. B) *Ex vivo* tumour volume was calculated with the following equation: A x B x C x π/6, where A, B, and C are the three tumour dimensions. * p< 0.05. C) Representative images of tumour size in each group.

### *3.5. Evaluation of the mechanisms involved in the reduction of tumour progression*

Since a decrease in tumour size was observed in the UVB1-treated group of mice in the HCT116 xenograft animal model, we decided to investigate the mechanisms underlying the tumour growth reduction. We studied the number of mitotic figures and the percentage of necrotic cells present in the slides of tumours stained with H&E and the expression of Ki-67, Bax, E-cadherin and β-catenin by immunohistochemistry (IHC). As shown in figure 5, no differences in the number of mitotic figures (figure 5A) and in the percentage of necrotic cells (data not shown) were found between tumours of the mice treated with the analogue with those treated with vehicle. In concordance with this result, Ki67 expression, a marker of proliferation, was similar in both groups (figure 5B). On the contrary, the expression of Bax, a marker of apoptosis, was increased in primary tumours of UVB1-treated compared with vehicle-treated animals (median IRS = 2.10 versus 0.17, respectively; p= 0.030; figure 5C).

Since a relationship between calcitriol and the epithelial to mesenchymal transition was recently demonstrated [40-42] and considering that the *in vitro* results showed that the analogue UVB1 reduced cell migration and invasion of HCT116 cell line and modulated

E-cadherin levels, we decided to investigate the expression of these proteins in the tumour tissues. As shown in figure 5D, UVB1 increases E-cadherin (median IRS = 1.69 versus 0.97; p= 0.004) and decreases nuclear β-catenin (median IRS = 2.10 versus 0.90; p= 0.015, figure 5E) expression in animal tumour tissues.

Figure 5

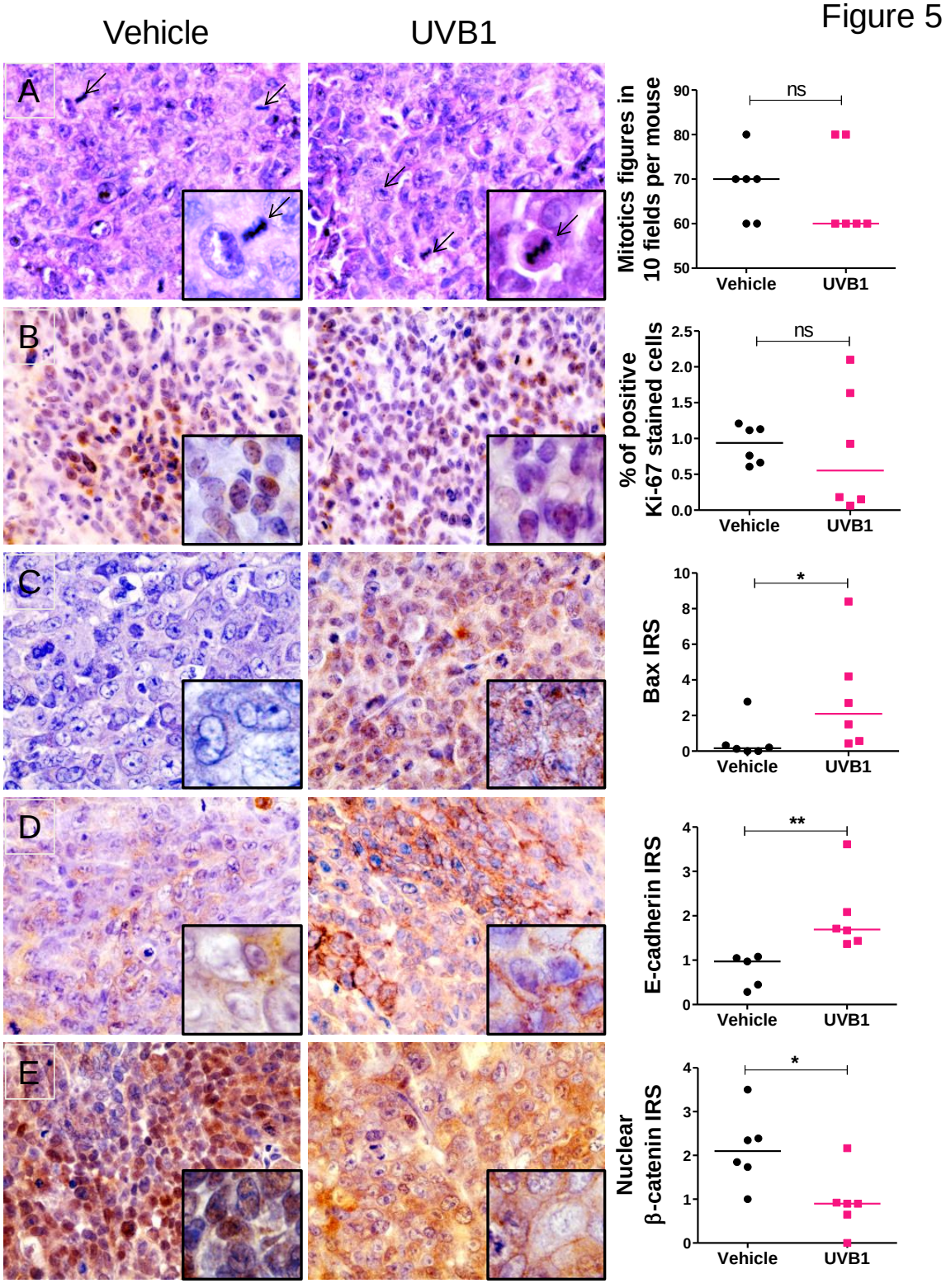


Figure 5. Analysis of the UVB1 and vehicle primary tumours of the xenograft animal model. Evaluation of A) mitotic index by H&E, B) Ki-67, C) Bax, D) E-cadherin and E) nuclear β-catenin expression by IHC in

s.c. primary tumours of HCT116 animal model. Immuno-Reactive-Score (IRS) was calculated as the product of the staining intensity by the percentage of positively stained cells. Representative micrographs of the tissues (×400 and ×1,000 for the inset) and parameter quantifications are shown; * $p< 0.05$, ** $p< 0.01$.

### *3.6. Effects of UVB1 on blood calcium levels, hematocrit and histology of organs of the animal model*

We had previously demonstrated that the administration of UVB1 to CF1 and nude mice did not produce hypercalcemia or toxic effects whereas calcitriol induced both hypercalcemia and the death of the animals during the treatment period [16]. We have now extended the analyses of the calcemic effects of the analogue studying a longer period of time. For this purpose, we tested the blood calcium levels in plasma obtained from the xenograft animal model treated with a 40 $\mu g.kg^{-1}$ of body weight of UVB1 during 30 days. As shown in figure 6A, UVB1 did not produce hypercalcemia. In addition, no changes in hematocrit (figure 6B), behaviour and body weight (figure 6C) were found. Furthermore, no alterations in animal histology of livers, kidneys and spleens were observed (figure 6D) at the end of the period of treatment.

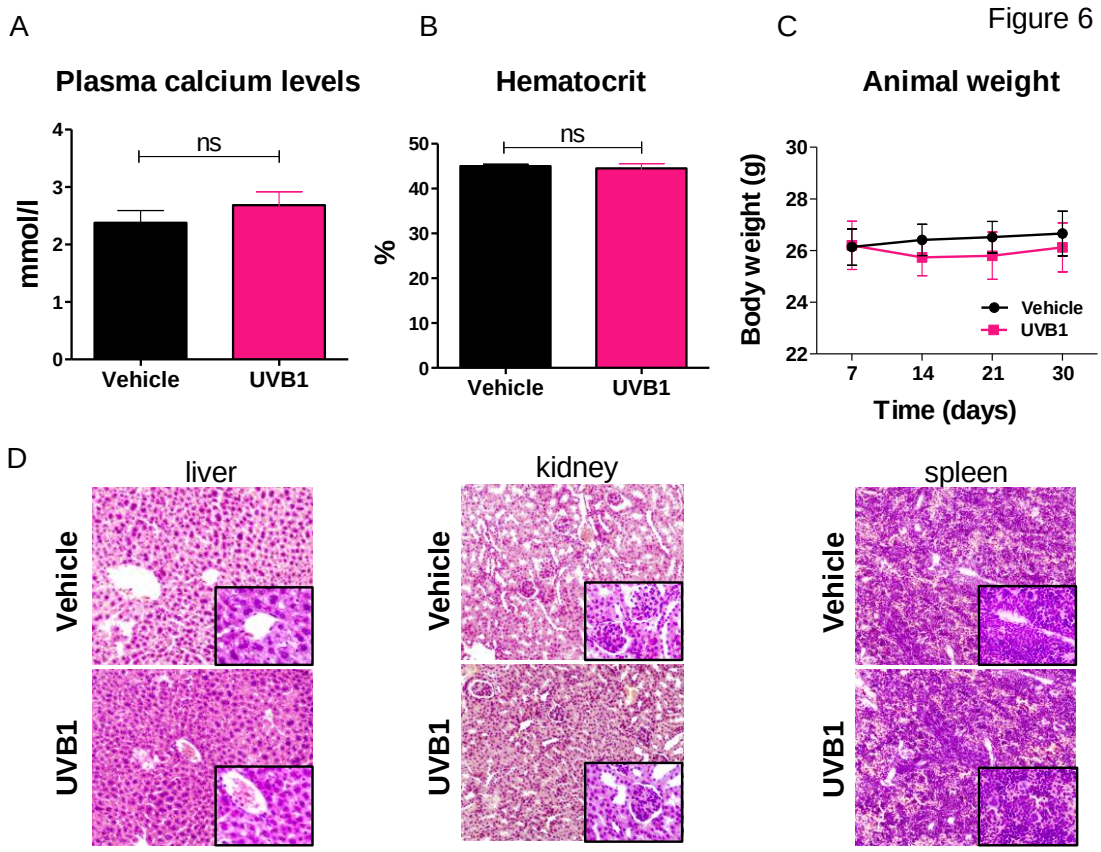


Figure 6

Figure 6. UVB1 effects on calcemic activity, hematocrit, body weight and histological examination of organs of the animal model. A) Plasma calcium levels, B) hematocrit, C) animal weight during the treatment and D) histological examination of livers, kidneys and spleens from N:NIH(S)-*Fox1*$^{nu}$ mice of the xenograft model treated with UVB1 and vehicle at the end of the treatment period.

### *3.7. Binding of UVB1 to VDR: Molecular modeling studies*

As described in the Introduction section, the genomic effects of calcitriol are mediated through the VDR. In order to study if the differential antitumour effects observed between UVB1 and calcitriol are due to a different interaction of these compounds with the VDR, we decided to study the interaction between UVB1 and the VDR LBD at a molecular level by applying computational techniques, such as molecular docking, molecular dynamics (MD) and free energy of binding analyses. A comparative study between UVB1 and calcitriol was performed in the search of intermolecular interaction patterns that may justify the above presented experimental observations.

#### *3.7.1. Molecular docking studies*

The crystal structure of the VDR LBD in complex with calcitriol has been previously reported by Rochel et al. [7], and considering that this structure corresponds to the bioactive conformation of VDR (i.e. contains an activated AF-2 domain), docking of UVB1 was performed on this crystallographic structure. Figure 7 presents the intermolecular interactions between calcitriol and VDR in the corresponding crystal structure and those interactions identified for UVB1 after molecular docking procedures were applied.

Figure 7

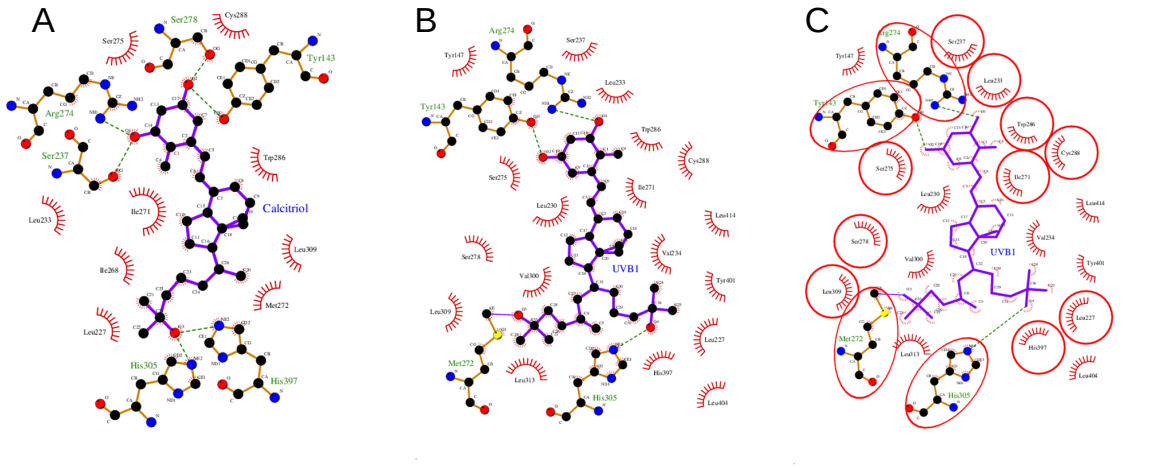


Figure 7. Molecular docking of UVB1 to crystal structure of the VDR LBD. A) Intermolecular interactions between calcitriol and VDR, B) Intermolecular interactions between the analog UVB1 and VDR obtained from docking studies and C) Intermolecular interactions with VDR shared between calcitriol and UVB1 (circles) and unique to UVB1 (plain).

Figure 7A depicts the interactions observed for the calcitriol: VDR complex, in which all interactions previously identified as critical for allosteric modulation of VDR were observed [7,22]. Interactions exhibiting particular relevance include a network of hydrogen bonds involving residues Ser237, Arg274, Ser278, Tyr143, His305 and His397. In addition, several Van der Waals interactions are established between calcitriol and residues Ser275, Cys288, Leu233, Ile271, Trp286, Ile268, Leu309, Met272 and Leu227 of VDR. With the exception of Ile268, all these residues also interacted with UVB1 (Figure 7B), while several additional Van der Waals interactions were present for the analogue, involving residues Tyr147, Val234, Leu404, Leu230, Leu313, Val300, Tyr401 and Leu414

(Figure 7C). These observations demonstrate that UVB1 is able to fit within the VDR ligand binding site, establishing homologous interactions to those observed for calcitriol, and thus eliciting an allosteric modulation of VDR.

To further study the affinity of UVB1 for VDR, as well as the structural effects on VDR upon UVB1 binding, explicit solvent MD simulations were carried out. Both calcitriol and UVB1 remained bound to the LBD throughout the 20 ns of MD trajectory. The overall interactions energies of each ligand are presented in Table 1 and Figure 8, respectively.

Table 1. Energetic components calculated for the intermolecular interaction between calcitriol and UVB1 with VDR.

| Component | Calcitriol (Kcal/mol) | UVB1 (Kcal/mol) |
|---|---|---|
| Van der Waals | -63.2 | -77.6 |
| Electrostatic | -28.5 | -24.2 |
| Gas | -91.7 | -101.8 |
| Polar solvation | 25.7 | 29.8 |
| Non polar salvation | -8.4 | -10.1 |
| Total | -74.4 | -82.1 |

Energetic components were calculated by means of explicit solvent MD simulations.

As can be seen in Table 1, UVB1 exhibited a lower total interaction energy compared to that of calcitriol, indicating its enhanced affinity for the LBD than that of the natural ligand. This feature is originated in a higher Van der Waals interaction component observed for UVB1. To further analyse the interaction patterns, the per-residue total interaction energy profiles as well as the differential affinity between calcitriol and UVB1 are presented in Figure 8.

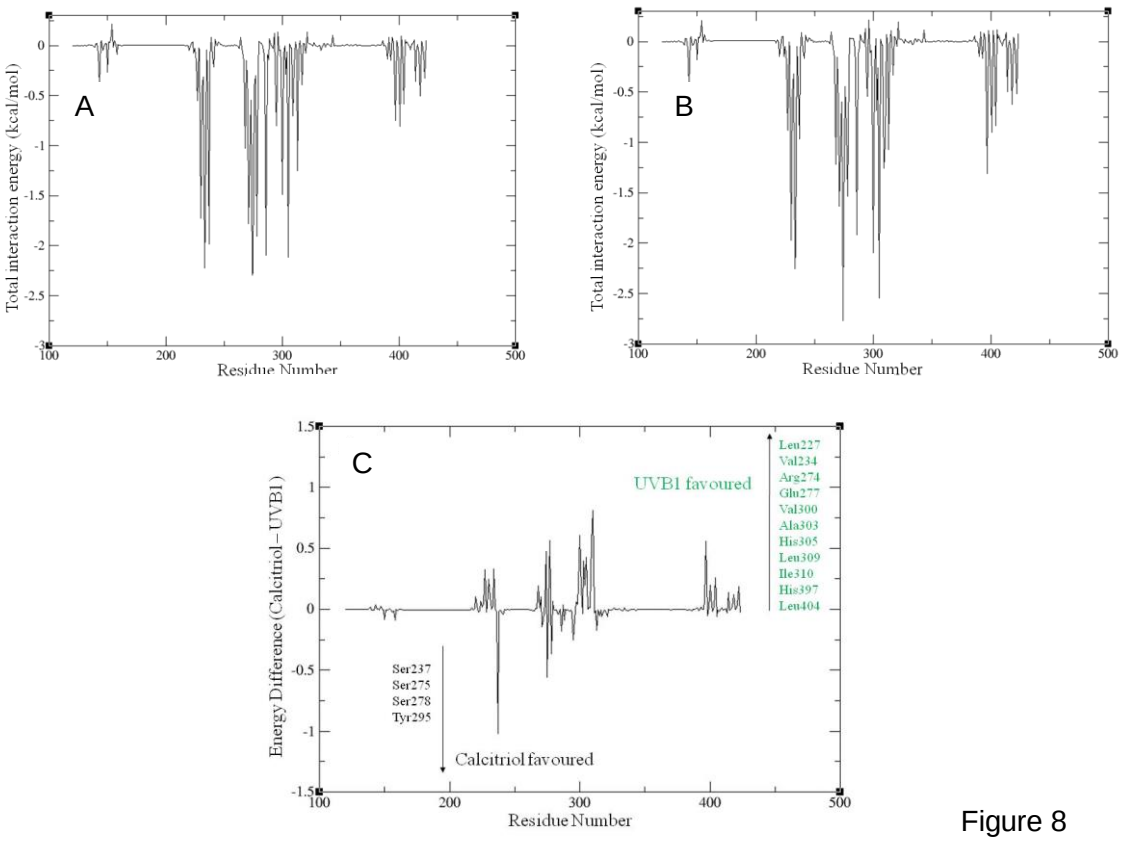


Figure 8

Figure 8. Per-residue intermolecular interaction patterns of UVB1 or calcitriol to VDR. A) Per-residue interaction energy decomposition for the calcitriol-VDR interaction, B) per-residue interaction energy decomposition for the UVB1-VDR interaction and C) per-residue calcitriol – UVB1 interaction energies demonstrating favoured contact points for each ligand.

As can be seen in Figures 8A and B, UVB1 exhibited a per-residue intermolecular interaction pattern similar to that of calcitriol, strongly suggesting a homologous binding mode of the former compound to the LBD. Figure 8C shows the per residue difference between interaction energies calculated for calcitriol and those found for UVB1. As can be seen, calcitriol exhibited an enhanced interaction with selected polar residues (Ser237, Ser275, Ser278 and Tyr295) compared to UVB1, while this last compound exhibited enhanced interactions with both polar (Arg274, Glu277, His305 and His397) and apolar (Leu227, Val234, Val300, Ala303, Leu309, Ile310 and Leu404) residues compared to calcitriol. As was previously mentioned, the higher binding affinity of UVB1 compared to calcitriol is mostly driven by the enhanced interaction with the above mentioned apolar residues of the VDR LBD.

To this point, the affinity of UVB1 for the VDR LBD was analysed. So, in order to further study the structural effects of UVB1 binding on the VDR three-dimensional structure, the atomic positional fluctuations (RMSF) were monitored throughout the MD simulation for H12, using as reference the initial (activated) crystallographic structure. Previous reports dealing with the allosteric activation of VDR have identified the conformational role of this loop for maintaining the functional AF-2 domain [7,22].

As can be seen in Figure 9A, UVB1 was able to maintain a similar conformational disposition on H12 as that elicited by calcitriol. This structural observation suggests that UVB1 is able to maintain an AF-2 conformation homologous to that observed for calcitriol, thus supporting the VDR-mediated antitumour effects of this new compound.

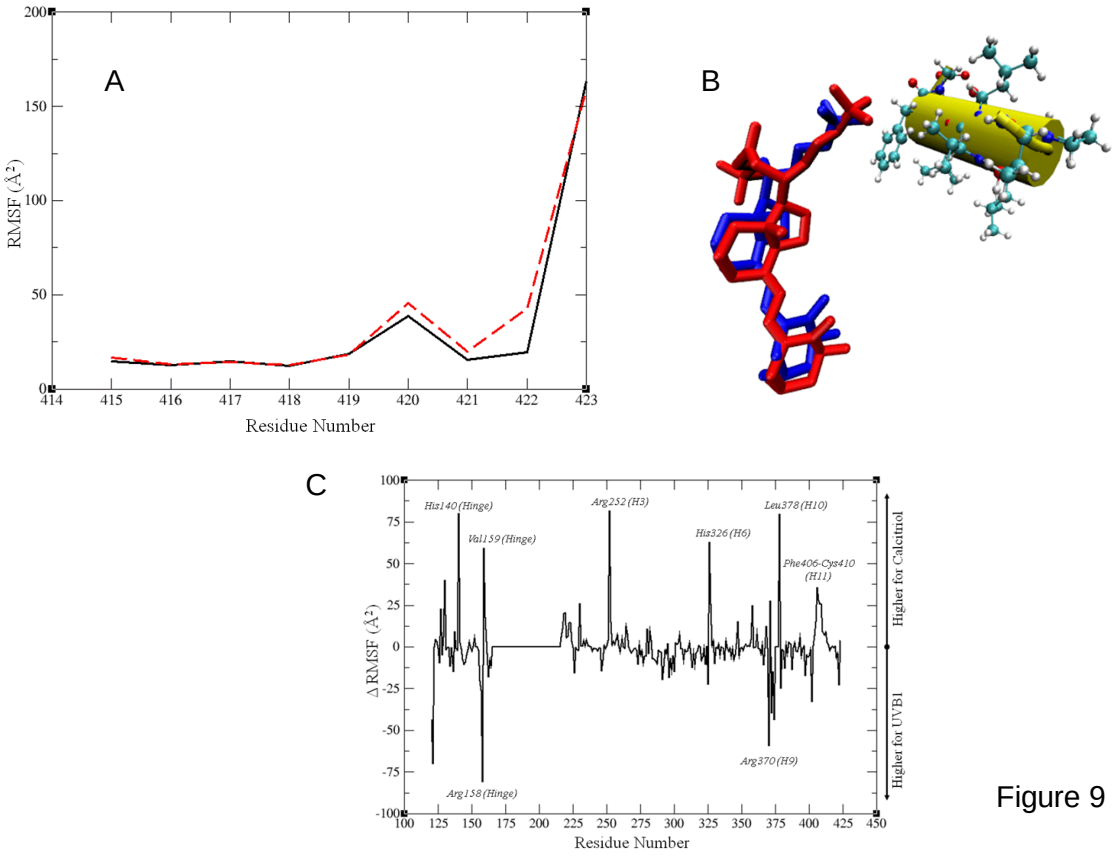


Figure 9

Figure 9. Atomic positional fluctuations (RMSF) monitored throughout the MD simulation for loop H12. A) RMSF relative to the crystallographic structure calculated for residues comprising H12 of VDR, obtained during MD trajectories for calcitriol (black) and UVB1 (red), B) Relative positions of calcitriol (blue) and UVB1 (red) to loop H12. C) Difference between the RMSF calculated for calcitriol and UVB1 over the whole VDR structure subjected to MD studies.

Finally, RMSF values were calculated for the whole structures corresponding to the calcitriol and UVB1 MD trajectories, with the differences in per-residue atomic fluctuations being computed (Figure 9C). As can be seen, several residues exhibit differences in their positional fluctuations when VDR is complexed with calcitriol or UVB1. It is noteworthy that UVB1, when compared to calcitriol, is able to restrict the positional fluctuations of two residues of the hinge region (His140 and Val159) and several ones corresponding to the LBD (Arg252, His326, Leu378 and Phe406-Cys410). Several reports have suggested that the hinge region may participate in facilitating the positioning of the LBD and modulate the accessibility of loop H12 for the recruitment of co-regulators [43]. Considering that ligands and DNA can act together to fine tune the VDR mediated regulation of gene expression [8], further studies may be required to assess if the structural features presented in Figure 9C may account for the stronger antitumour properties observed for UVB1, and particularly its low hypercalcemic effect.

## 4. DISCUSSION AND CONCLUSIONS

CRC is the third most commonly diagnosed cancer in males and the second in females, and ranks as the third leading cause of cancer mortality worldwide [10,11]. In an effort to better understand the molecular dysregulation that lead to the disease, CRC has recently undergone extensive molecular characterization. This characterization has revealed important oncogenes (e.g., KRAS, BRAF, PIK3CA), tumour suppressor genes (e.g., APC, TP53, PTEN) and signaling pathways that are critical for the development, survival, and progression of CRC cells. These genes are involved in major signaling pathways that have been linked to cancer, including the Wnt/β-catenin, MAPK, TGF-β and PI3K pathways [44]. Thus, agents that target these pathways have consequently been developed. However, patients who are characterized based on these molecular markers still show remarkable variability in terms of prognosis and response to therapy [45]. Therefore, many studies have addressed further sub-classifications of CRC, focusing on epigenetic factors and gene expression profiles [46,47]. This, in turn, has led to the search of new drugs which might contribute to individualized therapy.

The role of vitamin D in the prevention of colon cancers has been documented [6,48,49]. However, the use of vitamin D compounds in clinical trials for the treatment of malignancies is limited because of the hypercalcemia resulting from the required therapeutic doses [50,51]. Several analogues have been designed, synthesized and tested with the aim of obtaining a less hypercalcemic response while retaining their chemopreventive properties. We had previously demonstrated that the novel Gemini analogue of calcitriol UVB1 exerts considerable antitumour activity in various cell lines corresponding to different cancer types, while lacking hypercalcemic or toxic effects in mice [16]. In this work we have focused on the antitumour effects of this analogue in CRC. Interestingly, UVB1 decreased the tumour growth in the HCT116 xenograft animal model of colorectal cancer. This result was expected in light of our *in vitro* results which showed that UVB1 decreases the viability of HCT116 cancer cell line through induction of apoptotic cell death and differentiation (increase in E-cadherin) of carcinoma cells. This is in accordance with published data showing that apoptosis sensitization by calcitriol in colorectal adenoma and carcinoma cells involves the up-regulation of pro-apoptotic proteins [52,53].

Calcitriol is a well-known pro-differentiating hormone which regulates the activity of genes involved in cell differentiation. For example, in SW480 colon carcinoma cells, calcitriol promotes differentiation by inhibiting β-catenin signaling and inducing the expression of adhesion proteins such as E-cadherin, occludin, and vinculin [40]. We have demonstrated that the analogue UVB1 up-regulates VDR *in vitro,* increases E-cadherin both *in vitro* and in animal tissues and decreases nuclear β-catenin in primary tumours of UVB1-treated animals. These results are coincident with the mechanisms cited by Palmer and col. [40]: the binding of vitamin D receptor (VDR) to β-catenin precludes the formation of transcriptionally active β-catenin / T cell transcription factor (TCF) complexes in the cell nucleus, thus impairing gene expression and producing β-catenin re-localization at plasma-membrane adherent junctions as a consequence of calcitriol induced E-cadherin upregulation.

Calcitriol and its analogues appear as promising candidates for colon cancer treatment [6,54]. In colorectal cancer cell lines, VDR expression levels decrease with advanced stages of the disease [54]. Therefore it is important to identify therapeutic candidates that

increase VDR expression. In this regard, our results demonstrated a greater up-regulation of VDR with UVB1 than with calcitriol treatment. Moreover, our *in silico* studies of the interaction between UVB1 and VDR at the molecular level demonstrated that UVB1 is not only able to bind to the VDR ligand binding site, but also exhibits an enhanced affinity compared to that of calcitriol. Also, MD simulations were able to further explore the structural effects of calcitriol and UVB1 on the three dimensional conformation of VDR, identifying several particularities for the new synthetic analog, which may constitute an important structure-property relationship for the design of new calcitriol analogs with safe antitumour properties.

Related to this, there are several reports that analyzed the conformations induced in VDR by analogues of calcitriol, coactivator interactions and gene transcription. With regard to gemini analogues, Norman and col [55] reported a gemini analogue (1α,25-dihydroxy-21-(3-hydroxy-3-methylbutyl)vitamin D3) which binds less efficiently to VDR (38% compared to calcitriol), generates unique conformational VDR changes, stimulates gene transcription in ROS cells and inhibits clonal growth with similar or increased potency than calcitriol, depending on the cell line studied. In concordance with this, Herdick and col [56] demonstrated that the characterization of functional conformations of a nuclear receptor, such as the VDR after binding to various analogues, is insufficient for extrapolating their gene regulatory potential. They reported a gemini analog (Ro27–2310) that behaves in solution assays as a weak VDR agonist in mediating a interaction of VDR with any of the three coactivators of the SRC-coactivator family (SRC-1, TIF2, and RAC3) and then, in reporter gene or mammalian one-hybrid assays, has a higher potency than calcitriol. Most VDR ligands have been identified as agonists or pure or partial antagonists. Calberg and col [57] reported that gemini analogues can switch from an inverse agonist to a superagonist, when the cells are exposed to high coactivator levels. In this regard, Huet and col [58] have shown that the two analogues Gemini-0072 and Gemini-0097 induce an extra cavity within the VDR, recruit coactivator SRC-1 better than the parental gemini and act as VDR superagonists.

Taking into account that cell systems differ in their endogenous coactivator expression levels [57,59], it would be important the evaluation of the affinity of the tested analogue to VDR, transactivation potency and the antitumour effects in the same cell type in order to

correlate the in silico, in vitro and in vivo effects. Future experiments are aimed at testing these activities of UVB1 analogue in HCT116 colorectal cells.

In conclusion, the effects of UVB1 on controlling the growth of colorectal carcinomas are, at least in part, a result of an increase in p53-dependent apoptosis and an induction of differentiation. Furthermore, the inhibition of cell migration and invasion observed *in vitro* suggests that this calcitriol analogue may also have antimetastatic effects. Altogether these results and those demonstrating lack of hypercalcemic and other toxic effects suggest that UVB1 is a potentially effective chemotherapeutic agent for the treatment of colorectal carcinomas.

## ACKNOWLEDGMENTS

This work was supported by the Agencia Nacional de Promoción Científica y Tecnológica (ANPCyT, PICT 2012-0966) and the Consejo Nacional de Investigaciones Científicas y Técnicas (CONICET, PIP 112-201101-00556). María E Fermento, Eliana N Alonso and María J Ferronato are recipients of a fellowship from CONICET.

We acknowledge the GPGPU Computing Group from the Facultad de Matemática, Astronomía y Física (FAMAF), Universidad Nacional de Córdoba, Argentina, for providing access to computing resources.

## CONFLICT OF INTEREST

The authors declare no conflict of interest

## REFERENCES

1. Deeb K.K., Trump D.L., Johnson C.S. (2007) Vitamin D signalling pathways in cancer: potential for anticancer therapeutics. *Nat Rev Cancer*. 7(9):684-700, doi:10.1038/nrc2196.

2. Hanahan, D.; Weinberg, R.A. (2011) Hallmarks of cancer: the next generation. *Cell*. 144 (5). 646-674, doi: DOI 10.1016/j.cell.2011.02.013.

3. Salomón, D.G., Mascaró E., Grioli S.M., Ferronato M.J., Vitale C.A., Radivoy G.E. *et al*. (2014) Phosphonate analogues of 1α, 25 dihydroxyvitamin D3 are promising candidates

for antitumoural therapies. *Curr Top Med Chem*. 14 (21):2408-23, doi: 10.2174/1568026615666141208101418.

4. Díaz, L., Díaz Muñoz, M., García Gaytán, A.C., Méndez, I. (2015) Mechanistic Effects of Calcitriol in Cancer Biology. *Nutrients.* 7. 5020-5050, doi:10.3390/nu7065020.

5. Welsh, J. (2012) Cellular and molecular effects of vitamin D on carcinogenesis. *Arch Biochem Biophys*. 523(1):107-14, doi: 10.1016/j.abb.2011.10.019.

6. Pereira, F., Larriba, M.J., Muñoz, A. (2012) Vitamin D and colon cancer. *Endocr Relat Cancer*. 19(3):R51-71, doi: 10.1530/ERC-11-0388.

7. Rochel, N., Wurtz, J. M., Mitschler, A., Klaholz, B., Moras, D. (2000) The crystal structure of the nuclear receptor for vitamin D bound to its natural ligand. *Mol. Cell.* 5(1): 173-179, doi: http://dx.doi.org/10.1016/S1097-2765(00)80413-X.

8. Christakos, S., Dhawan, P., Verstuyf, A., Verlinden, L., Carmeliet, G. (2015) Vitamin D: Metabolism, molecular mechanism of action, and pleiotropic effects. *Physiol. Rev*. 96(1): 365-408, doi: 10.1152/physrev.00014.2015.

9. Huet, T., Laverny, G., Ciesielski, F., Molnár, F., Ramamoorthy, T.G., Belorusova, A.Y. *et al*. (2015) A vitamin D receptor selectively activated by gemini analogs reveals ligand dependent and independent effects. *Cell Reports*. 10(4): 516-527,doi: http://dx.doi.org/10.1016/j.celrep.2014.12.045.

10. GLOBOCAN. (2012) [Online] Available from http://globocan.iarc.fr/Pages/fact_sheets_population.aspx) [Accessed: 19th December 2015].

11. Siegel, R., Desantis, C., Jemal, A. (2014) Colorectal cancer statistics. *CA Cancer J Clin*. 64(2):104-17, doi: 10.3322/caac.21220.

12. Petersen, S.H., Harling, H., Kirkeby, L.T., Wille-Jørgensen, P., Mocellin, S. (2012) Postoperative adjuvant chemotherapy in rectal cancer operated for cure. *Cochrane Database Syst Rev*. 3:CD004078, doi: 10.1002/14651858.CD004078.pub2.

13. Shah, S., Islam, M.N., Dakshanamurthy, S., Rizvi, I., Rao, M., Herrell, R. *et al*. (2006) The molecular basis of vitamin D receptor and beta- catenin crossregulation. *Mol.Cell*. 21, 799–809, doi: 10.1016/j.molcel.2006.01.037.

14. Byers, S.W., Rowlands, T., Beildeck, M., Bong, Y.S. (2012) Mechanism of action of vitamin D and the vitamin D receptor in colorectal cancer prevention and treatment. *Rev Endocr Metab Disord*. 13(1):31-8, doi:10.1007/s11154-011-9196-y.

15. Hathcock, J.N., Shao, A., Vieth, R., Heaney, R. (2007) Risk assessment for vitamin D. *Am J Clin Nutr* .85(1):6-18.

16. Ferronato, M.J., Salomón, D.G., Fermento, M.E., Gandini, N.A., López Romero, A., Rivadulla, M.L. *et al*. (2015) Vitamin D analogue: potent antiproliferative effects on cancer cell lines and lack of hypercalcemic activity. *Arch Pharm (Weinheim).* 348(5):315-29, doi: 10.1002/ardp.201400448.

17. Ferronato M.J., Obiol D.J., Fermento M.E., Gandini N.A., Alonso E.N., Salomón D.G. *et al*. (2015) The alkynylphosphonate analogue of calcitriol EM1 has potent anti-metastatic effects in breast cancer. *J Steroid Biochem Mol Biol.* 154:285-93, doi: http://dx.doi.org/10.1016/j.jsbmb.2015.09.009.

18. Kim, H.Y., Ryu, J.H., Chu ,C.W., Son, G.M., Jeong, Y.I., Kwak, T.W., *et al*.(2014) Paclitaxel-incorporated nanoparticles using block copolymers composed of poly(ethylene glycol)/poly(3-hydroxyoctanoate). *Nanoscale Res Lett.* 9(1):525, doi: 10.1186/1556-276X-9-525.

19. Remmele,W., Stegner, H.E. (1987) Recommendation for uniform definition of an immuno-reactive score (IRS) for immunohistochemical estrogen receptor detection (ER-ICA) in breast cancer tissue. *Pathologe* 8, 138–140.

20. Facchinetti, M.M., Gandini, N.A., Fermento, M.E., Sterin-Speziale, N.B., Ji, Y., Patel, V. *et al*. (2010) The expression of sphingosine kinase-1 in head and neck carcinoma. *Cells Tissues Organs*. 192(5):314-24, doi: 10.1159/000318173.

21. Rose, P. W., Prlić, A., Bi, C., Bluhm, W. F., Christie, C. H., Dutta, S. *et al*. (2015) The RCSB Protein Data Bank: Views of structural biology for basic and applied research and education. *Nucleic Acids Res*. 43(D1): D345-D356, doi: 10.1093/nar/gku1214.

22. Malinska, M., Kutner, A., Woźniak, K. (2015) Predicted structures of new Vitamin D Receptor agonists based on available X-ray structures. *Steroids.* 104: 220-229. doi: 10.1016/j.steroids.2015.10.007

23. MarvinSketch v.6.31., ChemAxon Ltd., http://www.chemaxon.com

24. Frisch, M. J., Trucks, G. W., Schlegel, H. B., Scuseria, G. E., Rob, M. A., Cheeseman, J. R. *et al*. (2003). Gaussian 03.

25. Omega.2.4.3. OpenEye.Scientific.Software, Santa Fe, NM, http://www.eyesopen.com.

26. Hawkins, P. C. D., Nicholls, A. (2012) Conformer generation with OMEGA: Learning from the data set and the analysis of failures. *J. Chem. Inf. Model*. 52(11): 2919-2936, dx.doi.org/10.1021/ci300314k.

27. Fred.3.0.0 OpenEye.Scientific.Software, Santa Fe, NM, http://www.eyesopen.com.

28. McGann, M. (2011) FRED pose prediction and virtual screening accuracy. *J. Chem. Inf. Model.* 51(3): 578-596, doi: dx.doi.org/10.1021/ci100436p.

29. McGann, M. (2012) FRED and HYBRID docking performance on standardized datasets. J. Comput. *Aided Mol. Des.* 8(26): 1-10, doi: 10.1007/s10822-012-9584-8.

30. VIDA.4.2.1 OpenEye.Scientific.Software, Santa Fe, NM, http://www.eyesopen.com.

31. Laskowski, R. A., Swindells, M. B. (2011) LigPlot+: Multiple ligand-protein interaction diagrams for drug discovery. *J. Chem. Inf. Model.* 51(10): 2778-2786, dx.doi.org/10.1021/ci200227u.

32. Salomon-Ferrer, R., Case, D. A., Walker, R. C. (2013) An overview of the Amber biomolecular simulation package. *Wiley Interdisciplinary Reviews: Computational Molecular Science.* 3(2): 198-210, doi: 10.1002/wcms.1121.

33. Case, D. A., Berryman, J. T., Betz, R. M., Cerutti, D. S., Cheatham, I. T. E., Darden, T. A. *et al*. (2015). AMBER 2015, University of California, San Francisco.

34. Wang, J., Wolf, R. M., Caldwell, J. W., Kollman, P. A., Case, D. A. (2004) Development and testing of a general Amber force field. *J. Comput. Chem.* 25(9): 1157-1174, doi: 10.1002/jcc.20035.

35. Hornak, V., Abel, R., Okur, A., Strockbine, B., Roitberg, A., Simmerling, C. (2006) Comparison of multiple amber force fields and development of improved protein backbone parameters. *Proteins.* 65(3): 712-725, doi: 10.1002/prot.21123.

36. Miller Iii, B. R., McGee, T. D., Swails, J. M., Homeyer, N., Gohlke, H., Roitberg, A. E. (2012) MMPBSA.py: An efficient program for end-state free energy calculations. *J. Chem. Theor. Comput.* 8(9): 3314-3321, doi: doi: 10.1021/ct300418h.

37. Humphrey, W., Dalke, A., Schulten, K. (1996) VMD: Visual molecular dynamics. *J. Mol. Graph*. 14(1): 33-38.

38. Leyssens, C., Verlinden, L., Verstuyf, A. (2013) Antineoplastic effects of 1,25(OH)2D3 and its analogs in breast, prostate and colorectal cancer. *Endocr Relat Cancer*. 22;20(2):R31-47, doi: 10.1530/ERC-12-0381.

39. Larriba, M.J., Ordóñez-Morán, P., Chicote, I., Martín-Fernández, G., Puig, I., Muñoz, A. *et al*. (2011) Vitamin D receptor deficiency enhances Wnt/β-catenin signaling and tumour burden in colon cancer. *PLoS One*. 6(8):e23524, doi:10.1371/journal.pone.0023524.

40. Palmer, H.G., Gonzalez-Sancho, J.M., Espada, J., Berciano, M.T., Puig, I., Baulida, J. *et al*. (2001) Vitamin D(3) promotes the differentiation of colon carcinoma cells by the

induction of E-cadherin, the inhibition of beta-catenin signaling. *J Cell Biol*. 154:369–387, doi: 10.1083/jcb.200102028.

41. Palmer, H.G., Larriba, M.J., Garcia, J.M., Ordóñez-Morán, P., Peña, C., Peiró, S. *et al*. (2004) The transcription factor SNAIL represses vitamin D receptor expression, responsiveness in human colon cancer. *Nat Med.* 10:917–919, doi: 10.1038/nm1095.

42. Larriba, M.J., Martin-Villar, E., García, J.M., Pereira, F., Peña, C., de Herreros, A.G., *et al*. (2009) Snail2 cooperates with Snail1 in the repression of vitamin D receptor in colon cancer. *Carcinogenesis*. 30:1459–1468, doi:10.1093/carcin/bgp140.

43. Orlov, I., Rochel, N., Moras, D., Klaholz, B. P. (2012) Structure of the full human RXR/VDR nuclear receptor heterodimer complex with its DR3 target DNA. *EMBO J*. 31(2): 291-300, doi: 10.1038/emboj.2011.445.

44. Fearon, E.R. (2011) Molecular genetics of colorectal cancer. *Annu Rev Pathol*. 6:479–507, doi: 0.1146/annurev-pathol-011110-130235.

45. Martini, M., Vecchione, L., Siena, S., Tejpar, S., Bardelli, A. (2012) Targeted therapies: how personal should we go? *Nat Rev Clin Oncol*. 9:87–97, doi: 10.1038/nrclinonc.2011.164.

46. The Cancer Genome Atlas Network. (2012) Comprehensive molecular characterization of human colon and rectal cancer. *Nature*. 487(7407):330-337, doi: 10.1038/nature11252.

47. Budinska, E., Popovici, V., Tejpar, S., D'Ario, G., Lapique, N., Sikora, K.O. *et al*. (2013) Gene expression patterns unveil a new level of molecular heterogeneity in colorectal cancer. *J Pathol*. 231(1):63-76, doi: 10.1002/path.4212.

48. Spina C., Tangpricha V., Yao M., Zhou W., Wolfe M.M., Maehr H. *et al*. (2005) Colon cancer and solar ultraviolet B radiation and prevention and treatment of colon cancer in mice with vitamin D and its Gemini analogs. *J Steroid Biochem Mol Biol*. 97(1-2):111-120, doi: 10.1016/j.jsbmb.2005.06.003.

49. Bostick RM. (2015) Effects of supplemental vitamin D and calcium on normal colon tissue and circulating biomarkers of risk for colorectal neoplasms. *J Steroid Biochem Mol Biol*. 148:86-95, doi: 10.1016/j.jsbmb.2015.01.010.

50. Baron J.A., Barry E.L., Mott L.A., Rees J.R., Sandler R.S., Snover D.C. *et al*. (2015) A Trial of Calcium and Vitamin D for the Prevention of Colorectal Adenomas. *N Engl J Med*. 15;373(16):1519-30, doi: 10.1056/NEJMoa1500409.

51. Bikle D.D. (2014) Vitamin D and cancer: the promise not yet fulfilled. *Endocrine*. 46(1):29-38, doi:10.1007/s12020-013-0146-1.

52. Díaz, G.D., Paraskeva, C., Thomas, M.G., Binderup, L., Hague, A. (2000) Apoptosis is induced by the active metabolite of vitamin D3 and its analogue EB1089 in colorectal adenoma and carcinoma cells: possible implications for prevention and therapy. *Cancer Res.* 60(8):2304-12.

53. Barnes, J.D., Arhel, N.J., Lee, S.S., Sharp, A., Al-Okail, M., Packham, G. *et al*. (2005) Nuclear BAG-1 expression inhibits apoptosis in colorectal adenoma-derived epithelial cells. *Apoptosis.* 10(2):301-11, doi: http://dx.doi.org/10.1007/s10495-005-0804-8.

54. Stubbins, R.E., Hakeem, A., Núñez, N.P. (2012) Using components of the vitamin D pathway to prevent and treat colon cancer. *Nutr Rev*. 70(12):721-9, doi: 10.1111/j.1753-4887.2012.00522.x.

55. Norman, A.W., Manchand, P.S., Uskokovic, M,R., Okamura, W.H., Takeuchi, J,A., Bishop, J.E. *et al*. (2000) Characterization of a novel analogue of 1alpha,25(OH)(2)-vitamin D(3) with two side chains: interaction with its nuclear receptor and cellular actions. *J Med Chem*. 13;43(14):2719-30. doi: 10.1021/jm0000160

56. Herdick, M., Bury, Y., Quack, M., Uskokovic, M.R., Polly, P., Carlberg, C. (2000) Response element and coactivator-mediated conformational change of the vitamin D(3) receptor permits sensitive interaction with agonists. *Mol Pharmacol*. 57(6):1206-17.

57. Carlberg, C., Molnár, F. (2006) Detailed molecular understanding of agonistic and antagonistic vitamin D receptor ligands. *Curr Top Med Chem*. 6(12):1243-53, doi: 10.2174/156802606777864908.

58. Huet, T., Maehr, H., Lee, H.J., Uskokovic, M.R., Suh, N., Moras, D., Rochel, N. (2011) Structure-function study of gemini derivatives with two different side chains at C-20, Gemini-0072 and Gemini-0097. *Medchemcomm*. 2(5):424-429, doi:10.1039/C1MD00059D.

59. Germain, P., Iyer, J., Zechel, C., Gronemeyer, H. (2002) Co-regulator recruitment and the mechanism of retinoic acid receptor synergy. *Nature* 10;415(6868):187-92, doi:10.1038/415187a.

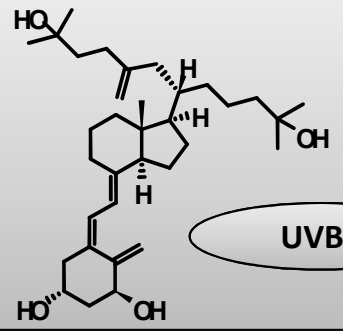


UVB1

**Vitamin D Analogue**

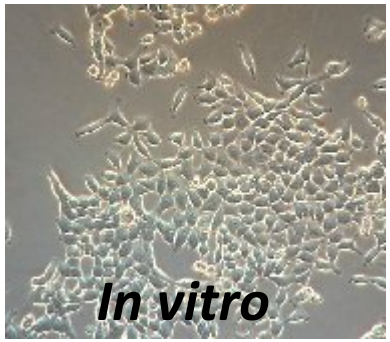



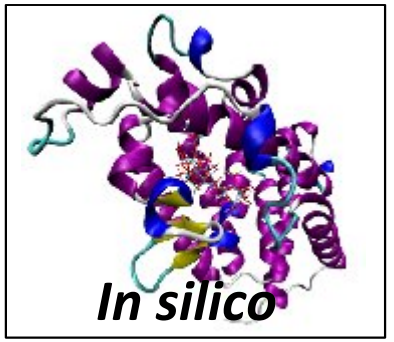


**Colorectal Cancer Progression**